

A family of fiber-optic based pressure sensors for intracochlear measurements

Elizabeth S. Olson^{*a}, Hideko H. Nakajima^b

^aDept. of Otolaryngology/Head&Neck Surgery and Biomedical Eng., Columbia U., New York NY;

^bDept. of Otology & Laryngology, Harvard Med. School, Mass. Eye & Ear Infirmary, Boston MA

ABSTRACT

Fiber-optic pressure sensors have been developed for measurements of intracochlear pressure. The present family of transducers includes an 81 μm diameter sensor employing a SLED light source and single-mode optic fiber, and LED/multi-mode sensors with 126 and 202 μm diameter. The 126 μm diameter pressure sensor also has been constructed with an electrode adhered to its side, for coincident pressure and voltage measurements. These sensors have been used for quantifying cochlear mechanical impedances, informing our understanding of conductive hearing loss and its remediation, and probing the operation of the cochlear amplifier.

Keywords: pressure sensor, fiber optic, cochlea, middle ear

1. INTRODUCTION

Fiber-optic pressure transducers were developed for measurements of intracochlear pressure. The first generation sensors were $\sim 146 \mu\text{m}$ in outer diameter (OD), which was reduced without complication to $\sim 126 \mu\text{m}$. A further reduction to $\sim 81 \mu\text{m}$ was achieved by adapting the light source (from light emitting diode (LED) to super-luminescent diode (SLED)) and fiber type (from multi-mode to single-mode). In another member of the family, the OD was increased to 202 μm , which simplified construction because hydrofluoric etching of the optic fiber insert was not needed. Finally, a dual pressure+voltage sensor was constructed by adhering an isonel-insulated platinum wire to a multi-mode pressure sensor.

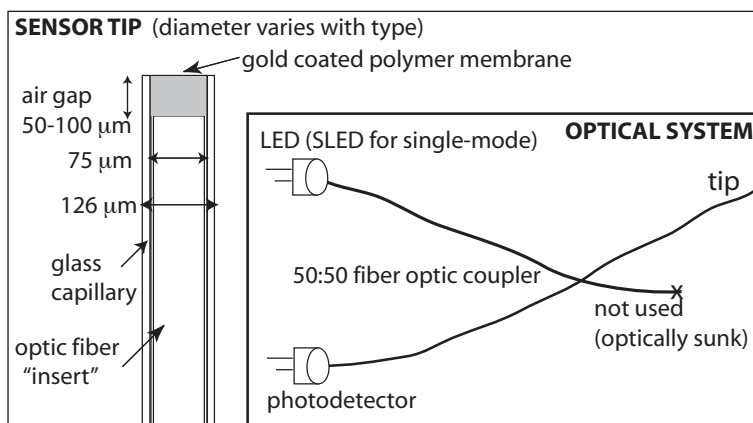


Figure 1. Sensor tip and diagram of optical system. The optic fiber insert, with starting diameter 125 μm , was etched for several hours in 8% hydrofluoric (HF) acid, reducing its diameter so that it would slide within the glass capillary. Threading is done under an operating microscope. Flat ends of optic fiber insert and glass capillary, and flat membranes are necessary for reasonable sensor sensitivity. To use the sensor, the tip assembly is threaded into a glass capillary protective housing (1 mm diameter, several cm long) whose tip has been pulled or melted down to limit lateral movement of the tip. This capillary is adhered to an aluminum rod that can be held in a micromanipulator.

In live rodents, the sensors have been used to map the intracochlear pressure field, and in concert with motion measurements, to determine the mechanical impedance of the cochlear partition and the input impedance of the cochlea. They have been used to explore middle ear transmission, distortion product generation and transmission, and the electro-mechanics of cochlear amplification.

In fresh cadaveric human temporal bones, the sensors have been used to measure the intracochlear pressure near the oval and round windows in order to determine the input pressure drive to the cochlea. Pressure drive was found for various types of stimulation (air conduction, bone conduction, round window prosthetic) and in various disease states (ossicular fixation, canal dehiscence). Simultaneous velocity measurements allowed for the quantification of cochlear mechanical impedances, and informed our understanding of how these impedances affect the efficacy of the different stimulation modalities.

The physiological findings were the focus of our previous research papers. Here we emphasize the sensors. We describe sensor construction, calibration, frequency response, stability, and linearity. We also show the utility of the sensors for precisely determining delay in interferometric systems. A list of physiological studies done with the sensors is in the conclusion.

2. SENSOR BASICS: CONSTRUCTION AND CALIBRATION

Table 1. Sensor components

Item	Multi-mode sensors	Single-mode sensor
Light source	Honeywell HFE4050 LED, 850 nm center wavelength, 60 nm bandwidth, 70 μ W power. With ST connector. (No longer manufactured, see e.g. OPTEK for alternatives.)	WT&T, Quebec. LD03-BB SLED, 1530 nm center wavelength, 50 nm bandwidth, 5 mW power. With FP/APC connector.
Photodetector	Honeywell HFD 3002 (no longer manufactured), or OPTEK OPF482. With ST connector.	Thorlabs FGA04 with FP/PC bulkhead connector.
Fiber coupler (In all cases 50:50 split). Suppliers: Gould fiber optics, Millersville, MA; Fiber Instrument Sales, Oriskany NY.	Multi-mode coupler composed of 50/125 fiber. When needed, sensor tip fiber HF etched to diameter \sim 5 μ m smaller than ID of tip.	Single-mode, wavelength flattened coupler. (Sensor tip end connected via FP/APC connector to 9/125 single-mode fiber, etched at distal end to fit into tip.)
Tips: PolymicroTechnologies (Phoenix, AZ) TSP series capillary. ID/OD (μ m), OD noted is after removing capillary's polymer coating.	TSP100170: ID/OD = 100/146 TSP75150: ID/OD = 75/126 TSP128226: ID/OD = 128/202	TSP40105: ID/OD = 40/81.
Dual sensor electrode: AM systems, Sequim WA	Isonel-insulated platinum wire, diameter .0011" with insulation.	Not made.

The optical components of the pressure sensor, diagrammed in Fig. 1, are a 50:50 optic fiber coupler, a wide-band light source and a photodetector. The pressure sensing tip comprises a short (\sim 1 cm) piece of capillary tubing (Polymicro Technologies, Phoenix AZ) capped at one end with a thin polymer membrane, with an evaporated gold coating covering the membrane. The membrane is made by floating UV-curing adhesive (Norland Products, Cranbury NJ) on water until broad regions of bright interference colors appear, at which point the adhesive is cured. The tip is then dipped through the floating membrane material. The thickness is \sim half the wavelength of the corresponding light, or \sim 0.3 μ m. Gold coating of the membrane is best done with an evaporator, rather than a sputterer, in order to reduce the amount of gold deposited on the side walls, because one needs to see through them when the fiber insert is threaded into the capillary. Also, in our experience sputtering often distorted the membranes. Cleaving of the optic fiber and the capillary tubing for the tip is done with a precision fiber optic cleaver. The blade adjustment allows cleaving of fibers of a variety of

diameters. A fiber optic fusion splicer is useful but not required. These components are available from fiber optic suppliers, for example Fiber Instrument Sales, Oriskany NY.

The sensors operate as optic levers – light emerges from the optic fiber insert, fans out and is reflected from the gold-coated membrane. The amount of light that returns to the fiber after reflecting from the membrane depends on the distance to the membrane and varies in step with pressure-induced membrane motion. This is how the sensor operates to detect pressure. [Another possible mode of operation would be due to interference between the membrane-reflected light and the light reflected off the flat surface of the optic fiber insert. For the LED-based system the interferometric-based signal is ruled out due to the short coherence length of the LED ($\sim 12 \mu\text{m}$, found as center-wavelength²/bandwidth) compared to the $\sim 50\text{-}100 \mu\text{m}$ cavity depth. (Because the light traverses back and forth across the cavity, the cavity depth is doubled for the comparison, and $12 \mu\text{m} \ll 100 - 200 \mu\text{m}$.) For the SLED-based system an interferometric-based signal is more of a possibility, given the slightly longer coherence length ($\sim 45 \mu\text{m}$) and slightly shallower cavity. Nevertheless, both the single and multi-mode systems appear to operate as optic levers.]

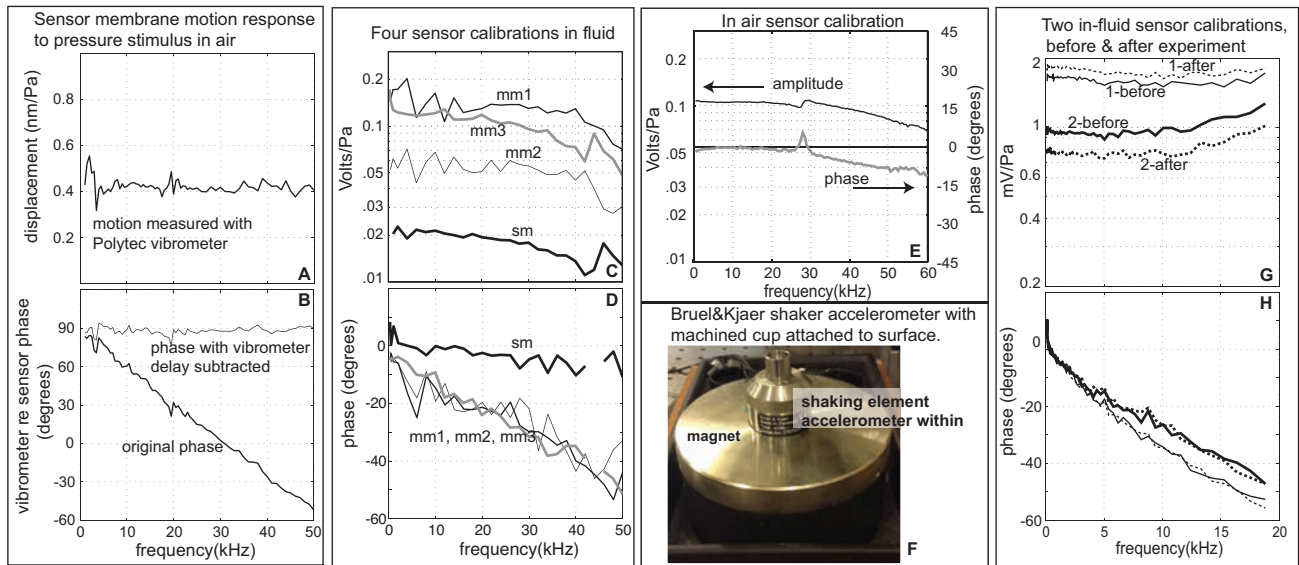


Figure 2. A. Sensor membrane motion measured with Polytec vibrometer. The vibrometer measures velocity and this was converted to displacement by dividing by radian frequency. B. Corresponding phase (vibrometer relative to sensor) before and after subtracting vibrometer delay. C. In-fluid sensor calibrations at Columbia. mm1, mm2 and mm3 were multi-mode sensors, sm was a single-mode sensor. mm1 and mm2 were calibrated one right after the other. D. Corresponding phase, relative to the shaker accelerometer. (The photodetector + amplifier circuitry varies between sensor types and is partly responsible for the sensitivity and phase differences between sensor types.) E. In-air calibration of multi-mode sensor. F. Shaker accelerometer used for in-fluid calibrations at Columbia; a similar unit is used at Mass Eye and Ear Infirmary (MEEI). G. In-fluid sensor calibrations at MEEI, before and after a temporal bone measurement. H. Corresponding phase.

Sensor stiffness: As described previously¹ stiffness of the sensor is partly due to membrane stiffness. For a clamped circular plate, the ratio of pressure to center displacement = $64D/r_0^4$, with r_0 the radius (inner radius of the sensor tip) and D the flexural rigidity, $D = Et^3/(12(1-\nu^2))$. ν is the Poisson's ratio, ~ 0.4 for typical plastics and E is the Young's modulus. $E = 0.14 \text{ GPa}$ for the membrane material (Norland optical adhesive #68) and for all the sensor types, $t \sim 0.3 \mu\text{m}$. From this, $D \sim 3.75 \times 10^{-13} \text{ Pa}\cdot\text{m}^3$. The membrane stiffness (in Pa/m) of the $100 \mu\text{m}$, $75 \mu\text{m}$, $128 \mu\text{m}$ and $40 \mu\text{m}$ ID sensor tips (see table 1) is calculated as $3.8 \times 10^6 \text{ Pa/m}$, $1.2 \times 10^7 \text{ Pa/m}$, $1.4 \times 10^6 \text{ Pa/m}$, $1.5 \times 10^8 \text{ Pa/m}$. A second, larger source of stiffness is due to compression of the air gap between the membrane and the inserted fiber. This is simply calculated by assuming either isothermal or adiabatic compression. In the isothermal case, $PV=\text{constant}$ ($V=\text{volume}$ of the cavity, area x depth), in the adiabatic case $PV^{1.4}=\text{constant}$, and with atmospheric pressure of 10^5 Pa and cavity depth of $100 \mu\text{m}$, the relationship between pressure variation and depth variation (due to membrane motion) is $\sim 10^9 \text{ Pa/m}$ or $1.4 \times 10^9 \text{ Pa/m}$. Stiffness scales inversely with cavity depth to the first power. Thus, the stiffness due to air compression dominates that of the membrane. A measurement of membrane displacement made with a Polytec vibrometer (VD06) is in Fig. 2A, and verified the expected displacement size, $\sim 0.4 \text{ nm/Pa}$. (The vibrometer measures velocity and this was converted to displacement by dividing by radian frequency.) The phase difference showed a relative delay of $7.8 \mu\text{s}$ and when this delay was subtracted from the results, the vibrometer phase led the sensor output by 90° , which was as

expected because the vibrometer measures velocity and the sensor's optic-lever operation measures displacement (and velocity leads displacement by 90°). Polytec gives an approximate $11 \mu\text{s}$ delay for the VD06, but does not provide a precise system-specific number. Fig. 2D shows a $\sim 2\text{-}3 \mu\text{s}$ sensor delay, thus the total VD06 delay is the sum, $\sim 11 \mu\text{s}$, as expected. Knowing the relative delay between the vibrometer and the sensor to high precision has been essential to studies relating motion to pressure^{2,3}.

Sensor calibration: As described and developed previously^{1,4}, fluid calibrations were done by providing a constant pressure stimulus over a wide range of frequencies, and measuring the sensor voltage. The pressure stimulus was created by immersing the sensor a prescribed distance (1-5 mm) beneath the surface of a vial of water, which was securely attached to a shaker + accelerometer (Bruel and Kjaer (B&K) type 4290, see Fig. 2F). The shaker was driven to accelerate it vertically with constant amplitude (and slightly decreasing with frequency to account for a standing wave induced pressure increase). Putting aside the small standing wave correction, pressure, $P = \rho ad$ ($d = \text{depth}$, $a = \text{acceleration}$, $\rho = \text{density of water} = 10^3 \text{ kg/m}^3$). With 1 mm immersion and 0.2 m/s^2 acceleration, $P = 0.2 \text{ Pa} = 80 \text{ dB SPL}$. Example of several in-water calibrations from Columbia are in Fig 2C. The primary message of the plot is that both the multi-mode and single-mode sensor types have sensitivities (V/Pa) that are reasonably well approximated by a single frequency-independent value (for each sensor). The several dB erratic variations are not meaningful – to see this, note that most of the variations evident in mm1 and mm2 are common to both sensors, and these sensors were calibrated one right after the other – thus these variations are not within the sensors, but rather due to the shaker's sensitivity to its precise position within the magnet, and small air bubbles in the water within the cup. The downturn above 40 kHz is more consistent, but because it is only a 6 dB reduction at 50 kHz, and the shaker's frequency response is less reliable at high frequencies (its own principal mechanical resonance is at 50-60 kHz) we have not accounted for it in our analyses. When necessary, calibrations were performed before and after at least one hour of fluid immersion to screen for sensors that were stable to within 2 dB. Fig. 2D shows the sensor phase relative to the acceleration, measured with the accelerometer housed within the shaker. The multi-mode sensor introduces a 2-3 μs delay over this frequency range. The delay is shorter for the single-mode sensors due to the different photodetector circuitry. The sensor phase delays are accounted for when necessary in analyses. Calibrations in air were also done, usually by inserting the sensor tip behind the protective grid of a B&K $\frac{1}{4}$ inch microphone, stimulating with sound free field and comparing the sensor to the B&K measurement. The air and fluid calibration values of a single sensor often agreed to within a few dB. Air calibrations were done at 27 and 37 C (room and body temperature) in order to screen out sensors with substantial temperature sensitivity. Fig. 2E shows an air calibration of a multi-mode sensor, performed in a machined cavity with a B&K 1/8 inch microphone providing the reference. The response is very smooth, with a frequency-dependent decrease amounting to 3 dB at 60 kHz. The small variation at $\sim 30 \text{ kHz}$ was due to the pressure field within the chamber.

The noise floor of the sensors is flat with frequency. For sensors like those of Fig. 2C&D it is at a level of $\sim -55\text{-}60 \text{ dBV}$ for the multi-mode sensors and -75 dBV for the single-mode sensors. The noise level is greater when the light returning to the photodetector is more intense, as expected when the noise is dominated by shot-noise in the photoelectric conversion. The signal:noise of the optical detection system increases with the square root of light level.

Fig. 2G&H shows a calibration of the $202 \mu\text{m}$ OD MEEI multi-mode sensors. Calibrations from two sensors are shown, before and after measurements in scala vestibuli (SV) and scala tympani (ST) of a cadaveric human temporal bone. The photodetector amplification and thus the V/Pa sensitivities are different from the Columbia multi-mode sensors. Many of the MEEI experimental analyses require a subtraction of pressures in the two scalae, in order to determine the pressure drive across the cochlear partition. When the analysis includes subtraction, a very reliable calibration is essential. This is in contrast to a measurement in which intracochlear pressure is related to ear canal (EC) pressure, for example. In the latter case, an error of 10 dB in calibration, although significant, will not change the frequency response or linearity of the results, which are usually the more critical aspects of the findings. In contrast, when the analysis requires a pressure subtraction, a 10 dB error in calibration will change the frequency response and possibly even the sign of the reported answer. Thus in most MEEI experiments, intracochlear pressure measurements were only used if the calibrations before and after cochlear insertion differed by less than $\sim 2 \text{ dB}$. Fig. 2G&H demonstrate that highly reliable and repeatable calibrations are possible before and after cochlear insertions and lengthy recording sessions.

Sensor linearity: Sensor output scaled linearly with pressure level to at least 60 Pa. This result was from a study of intracochlear responses at high stimulus level⁵. Using Fig. 2A, this would correspond to a membrane displacement of $\sim 25 \text{ nm}$.

Sensor problems: The main weakness of the pressure sensors is the stability of the calibration. In in-vivo experiments, pre and post experiment calibrations often differ by $\sim 6\text{-}10 \text{ dB}$. Sensitivity shifts occur at all frequencies, as a vertical

shift in sensitivity. The lack of stability of the sensors is related to their sensitivity and the fact that the membranes are positioned at the site of pressure measurement. Mechanical perturbation of the membrane redirects the light returning from the membrane, and thus changes the sensitivity. As noted above, in some cases this forced us to dismiss a data set, in others we made adjustments for the calibration uncertainty, for example by presenting results using several sensor calibrations⁶. However, we emphasize that screening for stable sensors before an experiment has allowed for measurements with calibration uncertainty of less than 1 dB. A less common instability is the phase of the sensor response. The sensors work by detecting the position of the pressure-sensitive membrane. When the membrane moves out and in, the light level returning to the fiber optic insert goes up and down (and ac voltage from the photodetector goes positive and negative). This indicates that the sensors work via a focusing or redirecting of light, so that when the membrane is pulled back, more of the light is directed to reenter the fiber optic insert. However, in ~ 1% of the multi-mode sensors the phase differs by 180° from the typical calibration phases (when this occurs it is for all frequencies). In rare cases, when the sensor is perturbed the phase will flip by 180° part way through an experiment. Although we can recognize and account for this behavior it is troubling to have this uncertainty. With the single-mode sensors the problem is more common. These are areas for improvement.

3. A SAMPLING OF RESEARCH FINDINGS

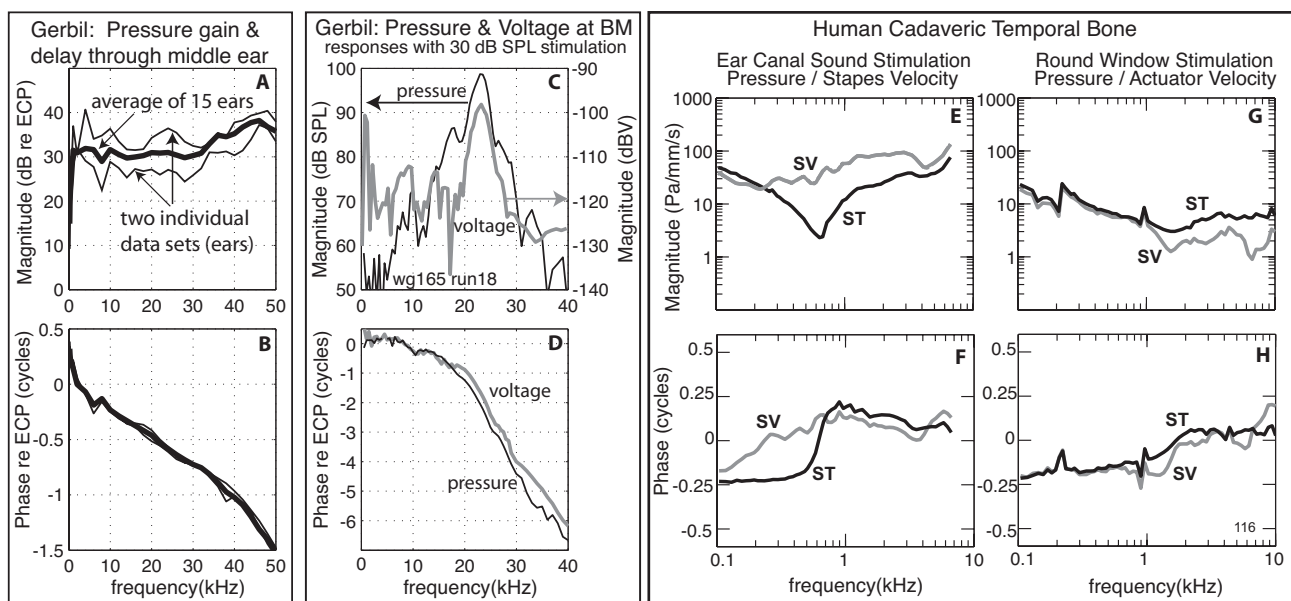


Figure 3. A&B. Ratio of SVP near the stapes to ECP. Average of responses in 15 preparations, and two individual responses. B. SVP – ECP phase. In these experiments both the EC and the SV pressure were measured with multi-mode pressure sensors. C&D. Dual-sensor pressure+voltage measurement. Pressure and voltage were measured 10 μ m from the basilar membrane (BM) in a sensitive healthy cochlea. Responses were measured over a range of stimulus levels and the 30 dB SPL result is shown here. D. Pressure and voltage phases relative to ECP phase. E-H. Temporal bone pressure measured in SV and ST. E-F. Stimulation was sound, delivered closed-field to the ear canal. G-H. Stimulation was via a piezoelectric actuator with smooth glass-rod tip that was coupled to the round window with a soft contact lens.

In Fig. 3 we show three examples of research findings that were made with the pressure sensors. Fig. 3 A&B are from the SV and EC pressure measurements that were part of an early study⁶. The flat frequency response and constant delay of the SVP/ECP ratio indicated that middle ear transmission in gerbil can be described as a frequency independent transmission line¹, as had been recently proposed in cat, based on EC pressure measurements⁷. This simple description of middle ear transmission was not expected, and we continue to work to understand how the complex motions of the eardrum and ossicles are able to provide such a beautiful and simple transmission profile. The study was enhanced by the fact that it used fiber-optic pressure sensors in the EC as well as in the cochlea. This allowed the ECP to be measured very close to the eardrum, and with a more accurate frequency response than with a probe tube microphone system. These benefits of using a pressure sensor in the EC were also apparent in the smooth responses observed in a study characterizing sound transmission through the middle ear in mouse⁸.

Fig. 3 C&D show data from a recent study in which pressure and extracellular voltage were measured simultaneously, close to the sensory tissue⁹. At low stimulus levels (the figure data were taken at 30 dB SPL) pressure and voltage tuning were pronounced and very similar, and both showed traveling wave phase delay. The simultaneity of the measurements allowed us to detect a phase shift of voltage relative to pressure, which occurred over a narrow frequency region just below the sharp peak (~17 kHz). In analysis, we linked the observed phase shift to activation of the cochlear amplifier – the active, outer-hair-cell-based electromechanical process that enhances cochlear responses in a place-frequency selective manner. With measurements of this sort we need to consider that the pressure sensor might perturb cochlear mechanics when it is close to the sensory tissue. However, in control measurements, perturbation due to the sensor is small^{6,10}.

Fig. 3 E&F show the magnitude and phase of pressure responses relative to stapes velocities evoked by sound stimulation at the EC¹¹, in human. Pressure in SV is much larger than in ST for most frequencies, as expected due to the low impedance that the volume velocity flow faces at the round window. In contrast, G shows that during round-window stimulation, the magnitudes of SV and ST pressure (recorded away from the BM) are similar over a wide frequency range. This is due to the volume velocity flow facing a high impedance at the oval window (stapes footplate). Although the pressure difference and neurophysiological measurements (for example, cochlear microphonic) can be the same for EC and round window stimulation, individual pressures in cochlear compartments are not the same, allowing us to understand how sound is transmitted to the cochlear partition by various means of stimulation.

4. CONCLUSION

Pressure is the stimulus for the ear and intracochlear pressure drives sensory tissue motion, leading to hair cell activation and hearing. Thus, intracochlear pressure is an essential quantity to measure and understand, and its measurement dates to the studies presented in 1980^{12,13}. The fiber optic pressure sensors presented here and used for the past ~ 20 years extended the study of intracochlear pressure due to their narrow diameter and wide-band response. They have been used in vivo and ex vivo in rodents to (i) measure middle ear transmission and cochlear input impedance^{1,2,8,14,15,16}, (ii) study transmission of sound in the EC and bulla^{17,18}, (iii) study bone conduction¹⁹, (iv) map intracochlear pressure²⁰, (v) study intracochlear distortion products and their relationship to emitted distortion products^{10,21,22,23}, (vi) measure pressure in the previously inaccessible scala media²⁴, (vii) quantify cochlear sensory tissue mechanics and electromechanics^{3,6,9,25}.

In fresh cadaveric temporal bones, the sensors have been used to (viii) measure the pressure drive across the basal cochlear partition upon EC air conduction²⁶, (ix) study prosthetic devices such as round-window stimulators^{11,27,28}, (x) study the effect of middle and inner ear pathology^{26,29,30}, (xi) understand and compare the transduction of sound for different types of stimulation¹¹.

ACKNOWLEDGEMENTS

We thank our lab-mates at Columbia and MEEI who contributed to sensor development and use, in particular Wei Dong and Mike Ravicz. Funding was provided by the NIH/ NIDCD and the Emil Capita Foundation.

REFERENCES

- [1] Olson, E.S., "Observing middle and inner ear mechanics with novel intracochlear pressure sensors," *J. Acoust. Soc. Am.* 103, 3445 – 3463 (1998).
- [2] de La Rochefoucauld, O., Decraemer, W.F., Khanna, S.M. and Olson, E.S., "Simultaneous measurements of ossicular velocity and intracochlear pressure leading to the cochlear input impedance in gerbil," *J. Assoc. Res. Otolaryn.* 9, 161 – 177 (2008).
- [3] Dong, W. and Olson, E.S., "In-vivo impedance of the gerbil organ of Corti at auditory frequencies," *Biophysical Journal* 97, 1233 – 1243 (2009).
- [4] Schloss, F. and Strasberg, M., "Hydrophone calibration in a vibrating column of liquid," *J. Acoust. Soc. Am.* 34, 958–960 (1962).
- [5] Huang, S., Dong, W. and Olson, E.S., "Subharmonic distortion in ear canal pressure and intracochlear pressure and motion," *J. Assoc. Res. Otolaryn* 13, 461– 471 (2012).

- [6] Olson, E.S., "Intracochlear pressure measurements related to cochlear frequency tuning," *J. Acoust. Soc. Am.* 110, 349 – 367 (2001).
- [7] Puria, S. and Allen, J.B., "Measurements and model of the cat middle ear: evidence of tympanic membrane acoustic delay," *J. Acoust. Soc. Am.* 104, 3463-3481 (1998).
- [8] Dong, W., Varavva, P. and Olson, E.S., "Sound transmission along the ossicular chain in common wild-type laboratory mice," *Hearing Research* 301, 27-34 (2013).
- [9] Dong, W. and Olson, E.S., "Detection of cochlear amplification and its activation" *Biophysical Journal* 105, 1067-1078 (2013).
- [10] Dong, W. and Olson, E.S., "Supporting evidence for reverse cochlear traveling waves," *J. Acoust. Soc. Am.* 123, 222-240 (2008).
- [11] Stieger, C., Rosowski, J.J., Nakajima, H.H., "Comparison of forward (ear-canal) and reverse (round-window) sound stimulation of the cochlea," *Hearing Research* 301, 105-114 (2013).
- [12] Dancer, A. and Franke, R., "Intracochlear sound pressure measurements in guinea pigs," *Hearing Research* 2:191-205 (1980).
- [13] Nedzelnitsky, V. "Sound pressures in the basal turn of the cat cochlea," *J. Acoust. Soc. Am.* 68, 1676-1689 (1980).
- [14] Ravicz, M.E., Slama, M.C., Rosowski, J.J., "Middle ear pressure gain and cochlear partition differential pressure in chinchilla," *Hearing Research* 263, 16-25 (2010).
- [15] Ravicz, M.E., Rosowski, J.J., "Inner-ear sound distribution near the base of the cochlea in chinchilla: further investigation," *J. Acoust. Soc. Am.* 133, 2208 – 2223 (2013).
- [16] de La Rochefoucauld, O., Kachroo, P. and Olson, E.S., "Ossicular motion related to middle ear transmission delay in gerbil," *Hearing Research* 270, 158 – 172 (2010).
- [17] Ravicz, M.E., Olson, E.S. and Rosowski, J.J., "Sound pressure distribution and energy flow within the gerbil ear canal from 100 Hz to 80 kHz," *J. Acoust. Soc. Am.* 122, 2154-2173 (2007).
- [18] Bergevin, C. and Olson, E.S., "External and middle ear sound pressure distribution and acoustic coupling to the tympanic membrane," *J. Acoust. Soc. Am.*, 135, 1294-1312 (2014).
- [19] Chhan, D., Roosli, C., McKinnon, M.L. and Rosowski, J.J., "Evidence of middle ear contribution in bone conduction in chinchilla," *Hearing Research* 301, 66-71 (2013).
- [20] Olson, E.S., "Direct measurement of intracochlear pressure waves," *Nature* 402, 526-529 (1999).
- [21] Dong, W. and Olson, E.S., "Two – tone distortion in intracochlear pressure." *J. Acoust. Soc. Am.* 117, 2999-3015 (2005).
- [22] Dong, W. and Olson, E.S., "Middle Ear Forward and Reverse Transmission in Gerbil." *J. Neurophysiol.* 95, 2951-2961 (2006).
- [23] Dong, W. and Olson, E.S., "Local cochlear damage reduces local nonlinearities and decreases generator-type cochlear emissions while increasing reflector type emissions." *J. Acoust. Soc. Am.* 127, 1422-1431 (2010).
- [24] Kale, S. and Olson, E.S. "Intracochlear pressure measurements in scala media inform models of cochlear mechanics," *Proceedings of the Mechanics of Hearing Meeting* (2014).
- [25] Olson, E.S., "Harmonic distortion in intracochlear pressure and its analysis to explore the cochlear amplifier." *J. Acoust. Soc. Am.* 115, 1230 – 1241 (2004).
- [26] Nakajima H.H., Dong W, Olson ES, Merchant SN, Ravicz ME, Rosowski J.J., "Differential intracochlear sound pressure measurements in normal human temporal bones." *J. Assoc. Res. Otolaryn.* 10, 23-36 (2009).
- [27] Nakajima, H.H., Dong, W., Olson, E.S., Merchant, S.N., Ravicz, M.E. and Rosowski, J.J., "Evaluation of round window stimulation using the floating mass transducer by intracochlear sound pressure measurements in human temporal bones" *Otology and Neurotology* 31, 506-511 (2010).
- [28] Nakajima, H.H., Merchant, S.N., Rosowski, J.J., "Performance considerations of prosthetic actuators for round-window stimulation," *Hearing Research* 263, 114-119 (2010).
- [29] Pisano, D.V., Niesten, M.E., Merchant, S., Nakajima, H.H., "The effect of superior semicircular canal dehiscence on intracochlear sound pressures," *Audiology & Neurotology* 17, 338-348 (2012).
- [30] Niesten, M.E., Stieger, C., Lee, D.J., Merchant, J.P., Grolman, W., Rosowski, J.J. and Nakajima, H.H., "Assessment of the effects of superior canal dehiscence location and size on intracochlear sound pressures," *Audiology & Neurotology* 20, 62-71 (2015).